

**Bonding and antibonding electromagnetic coupling in two interacting toroidal metamolecules**Tong Wu,<sup>1</sup> Andrey B. Evlyukhin<sup>2,3</sup>, and Vladimir R. Tuz<sup>1,4,\*</sup><sup>1</sup>State Key Laboratory on Integrated Optoelectronics, College of Electronic Science and Engineering, International Center of Future Science, Jilin University, 2699 Qianjin Street, Changchun 130012, China<sup>2</sup>Institute of Quantum Optics, Leibniz University Hannover, 30167 Hannover, Germany<sup>3</sup>Cluster of Excellence PhoenixD, Leibniz University Hannover, Welfengarten 1A, Hannover 30167, Germany<sup>4</sup>School of Radiophysics, Biomedical Electronics and Computer Systems, V. N. Karazin Kharkiv National University, 4 Svobody Square, Kharkiv 61022, Ukraine (Received 17 May 2024; revised 23 August 2024; accepted 23 August 2024; published 5 September 2024)

The existence of a toroidal-like eigenmode and its electromagnetic coupling in a system of dielectric particles are studied. A constituent structure (metamolecule) is made of a ring consisting of the radial arrangement of several vertically standing dielectric disks (meta-atoms). In the eigenstate of the given metamolecule, the second-order term related to the exact electric dipole in the multipole decomposition is much greater than the first-order term. This eigenstate is defined as a toroidal-like mode. Then, the characteristics of a system (metamacromolecule) composed of two identical rings are studied in both eigen- and excited states to reveal the peculiarities of the toroidal-like mode coupling. Similar to the well-known electric dipole-dipole and magnetic dipole-dipole interactions, the interaction of toroidal-like modes also appears in symmetric (bonding) and antisymmetric (antibonding) forms. Their excitation in the metamacromolecule depends on the propagation direction and polarization of the irradiating wave. The manifestation of toroidal-like mode coupling is confirmed by checking the extinction cross section and near-field distributions obtained from the full-wave numerical simulation and microwave experiment. A clear understanding of the nature of toroidicity is important from the fundamental physics perspective and practical implementation of metamaterials operated in such exotic states.

DOI: [10.1103/PhysRevB.110.115408](https://doi.org/10.1103/PhysRevB.110.115408)**I. INTRODUCTION**

In photonics, metamaterials are structured media, consisting of artificial “meta-atoms” or “metamolecules” ordered with a spatial resolution much smaller than the wavelength of light. The synthesis of such artificial structures is closely related to the principles of molecular modeling [1], which encompasses all theoretical and computational methods used to model or mimic the behavior of natural substances [2,3]. In their framework, meta-atoms of an artificial structure are designed to scatter the electromagnetic field in a prescribed manner, where their material properties and geometric shape contribute to the design parameters. Scattering characteristics of the meta-atoms are considered through the multipole expansion, based on which one can determine the polarizabilities of a substance and, therefore, its macroscopic parameters, such as permittivity, permeability, or index of refraction. The main goal of metamaterial engineering is to achieve properties that are rarely observed or even do not exist in natural substances [4].

Among the significant number of extraordinary properties that have been realized in metamaterials, artificial (optical) magnetism is perhaps the best known. The weak manifestation of magnetism at optical frequencies is a natural limitation, nevertheless, it can be realized by tailoring artificial meta-atoms to bear a magnetic response (it should be noted that in natural substances, magnetism is *static*, while in metamaterials, it is *dynamic*, caused by the reaction of particles to high-frequency electromagnetic radiation). In metallic meta-atoms, the magnetic dipole moment is realized by creating circular surface current flow in split-ring resonators [5], whereas, in dielectric ones, it originates from exciting specific electromagnetic modes of the particles with a circular displacement current flow of the field [6,7] (see, also, a comprehensive review [8] on the artificial optical magnetism). Combining particles into clusters to create metamolecules makes it possible to realize other related phenomena [9], in particular, a toroidal response due to electromagnetic coupling between the particles forming oligomers [10–14].

In natural materials known as multiferroics [15], toroidicity is associated with the magnetoelectric effect, where static toroidal moments appear in the electronic structure of several complex molecules [16,17]. In recent years, peculiarities of the manifestation of dynamic toroidicity in metamaterials have been widely discussed (see reviews [18,19] and references therein), noting that the toroidal response can be significantly enhanced in artificial structures compared to their natural counterparts. In addition to being of interest from the viewpoint of fundamental physics, artificial structures that

\*Contact author: tvr@jlu.edu.cn

support a toroidal response are also of significant practical importance, with promising prospects in the implementation of highly efficient sensors [20,21] and lasers [22].

In the framework of a general scattering theory, when implementing multipole expansion of the scattered field in terms of spherical harmonics [23,24], an exact electric dipole moment is expressed with the direct inclusion of the toroidal counterpart. In this approach, one shows that the toroidal multipoles are simple higher-order terms of an expansion of the spherical multipolar coefficients of electric parity. However, for certain structures, it is possible to obtain a response where the second-order term [toroidal dipole (TD) moment] in the expansion of the exact electric dipole moment dominates over the first-order one [quasistatic electric dipole (ED) moment] [25,26]. They are usually considered to be systems having a dynamic toroidal response [27,28].

Continuing the analogy with molecular physics, the effect of electromagnetic coupling between toroidal-like modes can be attributed to chemical bonding. Historically, chemical bonding was long formulated in terms of interactions between atoms [29]. Further, this approach has been developed to determine the electromagnetic interaction (hybridization) between two plasmonic nanoparticles [30,31] and their more complex ensembles [32,33], where the coupling originates from the electric dipole moments' interaction, acquiring symmetric (bonding) and antisymmetric (antibonding) configurations. The analogy between the atoms and their artificially created analogs was adopted to qualitatively and experimentally analyze the interaction between dielectric resonators, which are the building blocks of metamaterials, where both electric and magnetic dipole moments exist, determining the nature and strength of either electric dipole-dipole or magnetic dipole-dipole interactions [34–36]. Regarding the manifestation of toroidicity in metamaterials, the hybridization of certain modes in dielectric oligomers can also acquire bonding and antibonding configurations [37–41], resembling toroidal and antitoroidal orderings in multiferroics [42].

From the scattering theory perspective, a special technique (secondary multipole decomposition method [37,43]) should be further developed to find out how the multipole moments of the overall system, separate metamolecules, and their constituent meta-atoms are related to each other, resulting in the electromagnetic coupling of toroidal-like modes. Therefore, in the present paper, we modify this approach and study the manifestation of toroidicity in a metamolecule consisting of a ring system of disk-shaped dielectric resonators behaving as meta-atoms. First, we determine the toroidal-like mode from the solution to the eigenstate problem of the system by considering the magnitude of the toroidal contribution compared to the electric dipole one in the multipole decomposition. The issue of excitation of this eigenstate by the field of the incident wave is also discussed. Next, we consider electromagnetic coupling in a system of two metamolecules caused by the interaction of individual toroidal-like modes in each subsystem. We study this effect in both eigenstate and excited conditions. Finally, we present the results of our microwave experiment on the excitation of a single toroidal-like mode in the ring and measurements of their bonding and antibonding manifestations in a system of two closely spaced metamolecules to verify our findings.

## II. TOROIDAL-LIKE MODE OF A METAMOLECULE

### A. A metamolecule design

A classical model of the system sustaining a toroidal dipole moment is a wire helix (a solenoid) bent in a ring (a torus) [44]. A conducting wire is wrapped around the torus so that there are  $N$  turns between the entrance and the exit points for the uniform current flowing through the wire. This poloidal current creates a magnetic field trapped inside the torus. Equivalently, it can be represented by a closed loop of the head-to-tail arrangement of magnetic dipole moments. The resulting toroidal dipole moment of such a system is oriented along the axis of revolution of the torus (it is also known as a polar toroidal moment, where “polar” indicates that the moment transforms under parity as a polar vector [16]).

To imitate a toroidal response in an artificial structure, one could design a metamolecule supporting dynamically induced and spatially confined magnetization circulating along a loop. For dielectric structures, poloidal currents must be generated by displacement (polarization) currents. In this case, a metamolecule can be formed by several dielectric particles (meta-atoms) disposed close to each other, forming a ring, thereby promoting near-field coupling between the corresponding modes excited individually in each particle [12].

Therefore, in what follows, we consider a metamolecule made in the form of a ring consisting of the radial arrangement of  $N$  vertically standing disk-shaped dielectric particles, in such a way that they resemble wire coils (see the inset in Fig. 1). The metamolecule is characterized by a radius  $R$  related to the central line of the torus, whereas the constituent disks have the radius  $R_d$  and height  $H_d$ , respectively. These disks are made of a nonmagnetic material with the relative permittivity  $\varepsilon_d$ . For simplicity, but without loss of generality, we assume that the metamolecule is located in an airlike environment with the relative permittivity  $\varepsilon_s = 1$ .

Our study is carried out for the microwave range 1–20 GHz, considering our available laboratory means used for the experimental verification. In the chosen frequency range, the geometrical parameters of the structure are given on the millimeter scale. In order not to overload the study, we consider in the theoretical analysis that there are no material losses in the particles, while the effect of losses is revealed in our microwave experiment.

### B. Basic multipole expansion

Taking into account several first exact multipoles in the Cartesian basis, the scattering cross section of the metamolecule can be presented as [24,45]

$$\sigma_{\text{sca}} \simeq \frac{k_0^4}{6\pi \varepsilon_0^2 |\mathbf{E}|^2} |\mathbf{p}|^2 + \frac{k_0^6 \varepsilon_s}{720\pi \varepsilon_0^2 |\mathbf{E}|^2} \sum_{\alpha\beta} |Q_{\alpha\beta}|^2 + \frac{k_0^4 \varepsilon_s \mu_0}{6\pi \varepsilon_0 |\mathbf{E}|^2} |\mathbf{m}|^2 + \frac{k_0^6 \varepsilon_s^2 \mu_0}{80\pi \varepsilon_0 |\mathbf{E}|^2} \sum_{\alpha\beta} |M_{\alpha\beta}|^2, \quad (1)$$

where  $k_0$  is the wave number in vacuum,  $\varepsilon_0$  is the vacuum dielectric constant,  $\varepsilon_s$  is the relative dielectric constant of the surrounding medium,  $\mu_0$  is the vacuum permeability,  $\mathbf{E}$  is the electric field amplitude of the incident plane wave,  $\mathbf{p}$  and  $\mathbf{m}$  are the vectors of the exact electric and magnetic dipole

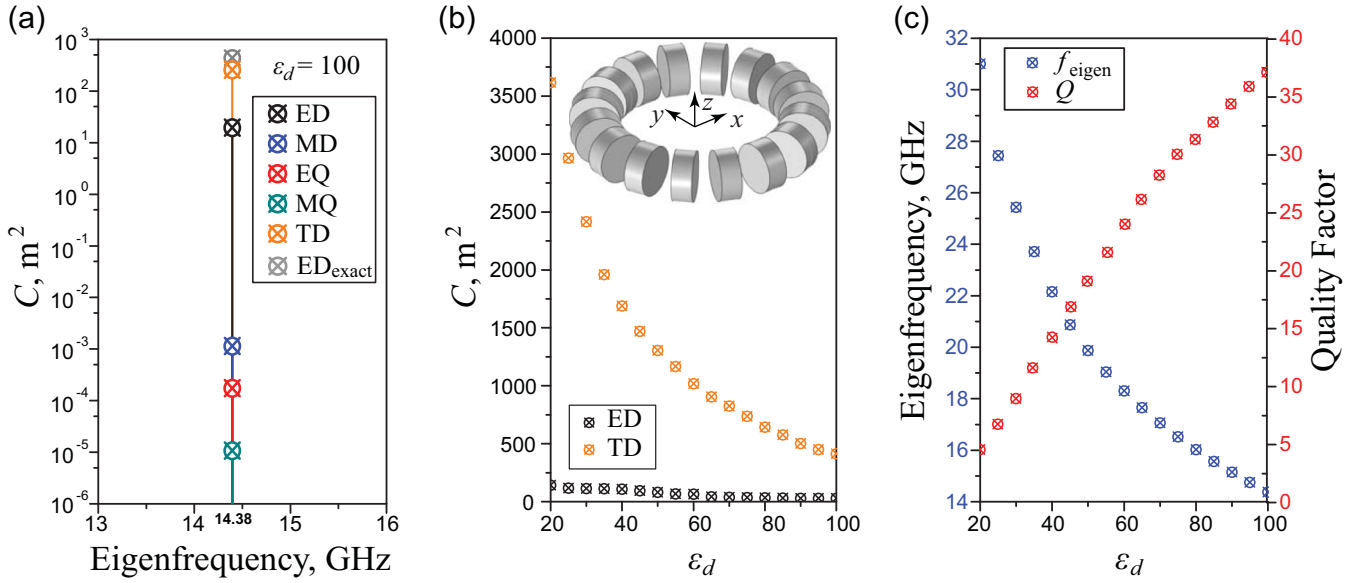


FIG. 1. (a) Contributions ( $C$ ) of the electric dipole (ED), magnetic dipole (MD), toroidal dipole (TD), electric quadrupole (EQ), magnetic quadrupole (MQ), and total exact electric dipole ( $\text{ED}_{\text{exact}}$ ) moments to the radiation power of the toroidal eigenstate given on the logarithmic scale. (b) The contributions of the ED and TD moments to the radiation power of the toroidal eigenstate, and (c) its eigenfrequency ( $f_{\text{eigen}}$ ) and quality factor ( $Q = \omega'/2\omega''$ , where  $\omega = 2\pi f_{\text{eigen}}$ ) as functions of the permittivity ( $\epsilon_d$ ) of the disk-shaped particles forming a metamolecule. Inset: The metamolecule design and Cartesian coordinate frame related to the problem. Geometrical parameters of the metamolecule are  $R = 4.0$  mm,  $R_d = 1.0$  mm,  $H_d = 0.8$  mm, and  $N = 16$ .

moments, respectively, and  $\hat{Q}$  and  $\hat{M}$  are the  $3 \times 3$  tensors of the exact electric and magnetic quadrupole moments (the integral expressions determining the exact multipole moments are not presented here and can be found in Table 2 in Ref. [24]).

For the scatterer that is smaller than the incident wavelength  $\lambda$  (in our problem, it can be related to the ring's diameter,  $2Rk_0\sqrt{\epsilon_s} \lesssim 1$ ), the expressions for the exact multipoles can be represented in the long-wavelength multipole approximation (LWA) [28],

$$\begin{aligned} \sigma_{\text{sca}} &\simeq \frac{k_0^4}{6\pi\epsilon_0^2|\mathbf{E}|^2} |\mathbf{p}_0|^2 + \eta |\mathbf{T}|^2 + \frac{k_0^6\epsilon_s}{720\pi\epsilon_0^2|\mathbf{E}|^2} \sum_{\alpha\beta} |Q_{\alpha\beta}^0|^2 \\ &+ \frac{k_0^4\epsilon_s\mu_0}{6\pi\epsilon_0|\mathbf{E}|^2} |\mathbf{m}_0|^2 + \frac{k_0^6\epsilon_s^2\mu_0}{80\pi\epsilon_0|\mathbf{E}|^2} \sum_{\alpha\beta} |M_{\alpha\beta}^0|^2 \\ &\equiv (\text{ED} + \text{TD}) + \text{EQ} + \text{MD} + \text{MQ}, \end{aligned} \quad (2)$$

where  $\eta = ik_0\epsilon_s c^{-1}$ , and ED, TD, EQ, MD, and MQ are the electric dipole, toroidal dipole, electric quadrupole, magnetic dipole, and magnetic quadrupole moments, respectively.

In the LWA, we omit the higher-order terms (the mean-square radii) for all contributions, while the electric  $\mathbf{p}_0$  and toroidal  $\mathbf{T}$  dipole moments, respectively, are expressed as

$$\mathbf{p}_0 = \frac{i}{\omega} \int_V \mathbf{J}_D d\mathbf{r}, \quad (3)$$

$$\mathbf{T} = \frac{1}{10} \int_V [(\mathbf{r} \cdot \mathbf{J}_D)\mathbf{r} - 2r^2\mathbf{J}_D] d\mathbf{r}, \quad (4)$$

where  $V$  is the total volume of the particles in the system,  $\omega$  is the angular frequency of the incident wave, and the time dependence  $\exp(-i\omega t)$  is assumed. For the system composed of  $N$  disks,  $V = \sum_{n=1}^N V_n$ , where  $n$  is the index running over

the disks. Explicit definitions of the rest of the multipoles entering the LWA can be found in Table 1 of Ref. [43]. We should emphasize that in the LWA, a TD moment arises as part of the total exact electric dipole moment ( $\text{ED}_{\text{exact}}$ ) [24].

For our calculation, we use the commercial COMSOL MULTIPHYSICS finite-element electromagnetic solver. The simulation model is based on the solution available from the COMSOL Application Gallery [46]. The spherical computational domain of our model includes the structure placed in a surrounding space truncated by a perfectly matched layer (PML). The PML is added to the model to simulate open (infinite) space and prevent unwanted re-reflections of waves within the computation domain. The origin of the Cartesian coordinate system coincides with the center of the torus. The equations of the multipole decomposition method are implemented in the solver as the computation procedures. We utilize the equations given in both exact form and long-wavelength approximation.

In our simulation procedure implemented in COMSOL, we first calculate the induced displacement current density  $\mathbf{J}_D(\mathbf{r})$  in the disks and then the total scattering cross section without application of the multipole decomposition method, and second, using the obtained  $\mathbf{J}_D(\mathbf{r})$ , the multipole moments and their contributions to the scattering cross section are determined in the LWA conditions.

### C. Eigenstate analysis

We start our research by examining the eigenstates of the given system. In this study, the multipole decomposition for each discrete eigenstate released by the solver is performed by integrating the mode eigenfield over the structure volume. We compare the magnitude of the TD moment against those of other dipole and quadrupole moments. We have defined the

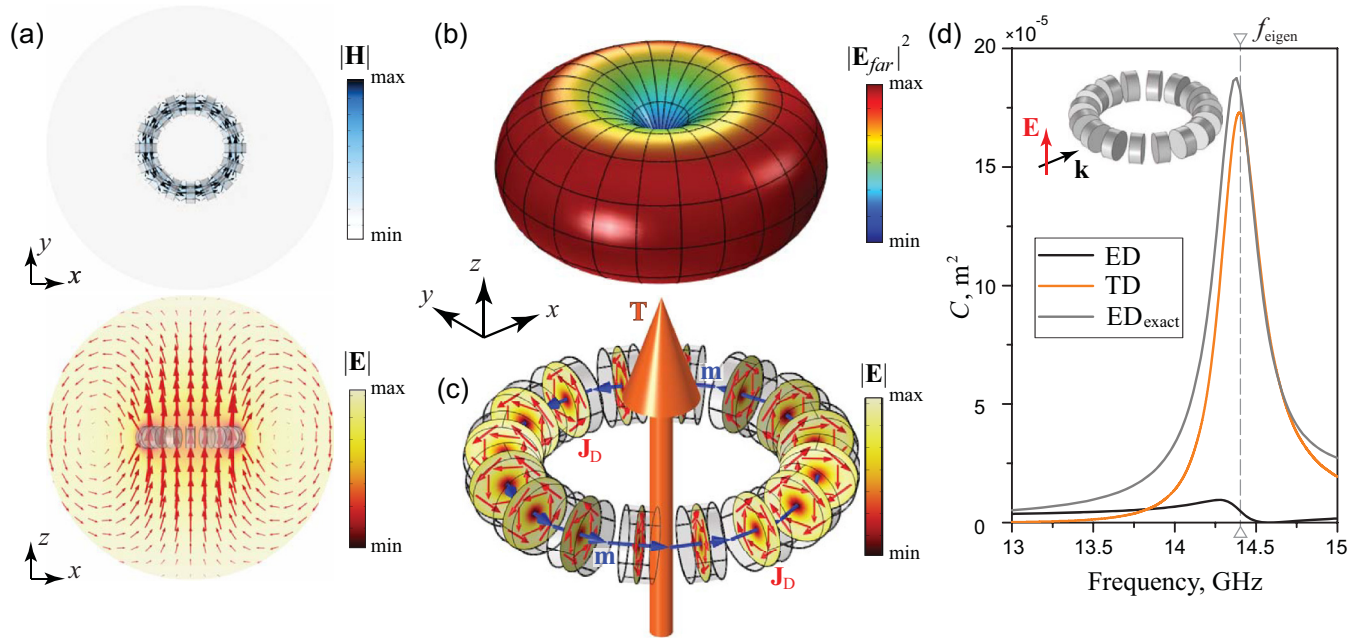


FIG. 2. (a) The magnitude and flow of the magnetic (cold color map, black arrows) and electric (hot color map, red arrows) near fields and (b) the far-field diagram of the toroidal eigenstate. (c) Schematic representation of the displacement current flow ( $\mathbf{J}_D$ , red arrows), individual MD moments ( $\mathbf{m}$ , blue arrows) of constituent meta-atoms, and TD moment ( $\mathbf{T}$ , orange arrow) of the toroidal eigenstate of the metamolecule. A hot color map presents the magnitude of the electric near field plotted at the vertical cross section of each disk. (d) The magnitude of the contributions to the scattering cross section of the total exact ED moment and ED and TD moments calculated in the long-wavelength approximation (LWA) for the metamolecule irradiated by a plane electromagnetic wave. Inset: The incidence condition and polarization of the wave. All geometric parameters of the metamolecule are the same as in Fig. 1, and  $\epsilon_d = 100$ .

toroidal-like mode of the structure ( $f_{\text{eigen}} = 14.38$  GHz) as a state for which the magnitude of the second-order term (TD moment) is much greater than that of the first-order term (ED moment), with negligible contributions from the remaining components in the decomposition [Fig. 1(a)].

To further reveal the peculiarities of the toroidal-like mode of the metamolecule, we subject it to a parametric study for the permittivity  $\epsilon_d$  of the constituent particles when all geometrical parameters of the system are fixed. We check the changes in the magnitude of the contributions of the ED and TD moments, eigenfrequency, and quality factor of the mode when permittivity varies in the range of  $\epsilon_d \in [20, 100]$ . Our calculations show that the difference between the TD and ED contributions increases with decreasing  $\epsilon_d$ , which is explained by the deterioration of the localization of the field inside the torus [Fig. 1(b)]. It is significant that at large  $\epsilon_d$ , the magnitude of the ED moment approaches zero (in the limit, this mode can be correlated with the toroidal mode of the first type with index  $m = 0$ , obtained for a toroidal cavity with a perfectly conducting wall; see Fig. 5 in Ref. [47]). As expected, a decrease in  $\epsilon_d$  is also accompanied by an increase in the eigenfrequency and a decrease in the quality factor of the mode [Fig. 1(c)]. It should be noted that a further decrease in  $\epsilon_d$  takes the model out of valid LWA conditions (the model is fully valid in quasistatic conditions where the size of the metamolecule is much smaller than the wavelength [44] and with the assumption that a uniform current is induced in each meta-atom which does not hold for small  $\epsilon_d$ ). Therefore, in what follows, we consider the characteristics of the structure at a relatively large  $\epsilon_d$ .

The solver allows us to visualize the eigenfield of the mode localized within the system. The patterns calculated for the toroidal-like mode show that the magnetic field is strongly localized inside the torus having a circular flow, while the electric field flow is indistinguishable from the distribution produced by the conventional electric dipole [Fig. 2(a)], which is fully consistent with the known properties of the toroidal state. The far-field radiation properties of the toroidal-like mode are also identical to those of the ED [Fig. 2(b)], as the electromagnetic theory suggests [18].

The nature of the toroidal-like mode is also confirmed by the arrangement of vectors of the displacement currents ( $\mathbf{J}_D$ ), corresponding MD moments ( $\mathbf{m}_j$ ) in each meta-atom ( $j = 1 \dots N$ ), and TD moment ( $\mathbf{T}$ ) of the entire metamolecule [Fig. 2(c)] (to calculate the MD moment of each particle within the secondary multipole decomposition method [37,43], we transfer the origin of the local coordinate system to the center of mass of the corresponding particle; see the Appendix). In particular, one can conclude that in each meta-atom, the lowest-order transverse electric (TE) mode of the cylindrical cavity is maintained (TE $_{01\ell}$  mode; see the mode nomenclature of the disk-shaped resonators in Ref. [48]). The TE $_{01\ell}$  mode is characterized by a circular flow of the displacement current that produces the MD moment directed along the axial axis of the disk. These individual TE $_{01\ell}$  modes of the meta-atoms are electromagnetically coupled in the metamolecule, producing its collective (hybrid) mode. Since disks are vertically standing, their MD moments acquire a head-to-tail arrangement, forming a ring along the central torus line. This configuration of MD moments is considered a

manifestation of the toroidal-like mode of a system [15], which is confirmed by the orientation of the overall TD moment of the metamolecule directed along the axis of revolution of the torus.

#### D. Toroidal-like mode excitation

The linearly polarized wave can interact with the toroidal mode when the direction of its electric field vector  $\mathbf{E}$  coincides with the vector  $\mathbf{T}$  belonging to the mode [18]. Further, for definiteness, we assume lateral irradiation of the metamolecule by a plane electromagnetic wave propagated along the  $x$  axis ( $\mathbf{E} = \{0, 0, E_z\}$ ,  $\mathbf{k} = \{k_x, 0, 0\}$ ,  $k = 2\pi f/c = \omega/c$ , where  $\omega$  and  $c$  are the angular frequency and speed of light in vacuum, respectively). In the simulation, a frequency sweep is performed in the range  $f \in [13, 15]$  GHz, which is chosen so that the eigenfrequency  $f_{\text{eigen}}$  of the toroidal-like mode lies within it. The obtained results show that the toroidal-like mode of the metamolecule is excited by the incident wave, providing the magnitude of the TD moment remains dominant compared to other multipole contributions, including the magnitude of the ED moment [Fig. 2(d)], where the resonant peak of the TD contribution coincides with the eigenfrequency of the mode.

### III. TOROIDAL DIPOLE COUPLING IN A METAMACROMOLECULE

#### A. A metamolecule pairing

In this section, we focus on the near-field interaction (hybridization [32]) of two identical toroidal metamolecules. Drawing an analogy with molecular physics, the system of two given rings can be associated with a “metamacromolecule.” When approaching two metamolecules bearing the toroidal-like modes to a sufficiently short distance, an efficient electromagnetic interaction mechanism between the modes of the rings is expected to occur, which is a subject of our subsequent study. We determine that the distance between metamolecules in the system is  $D$ , measured from the center of the rings, while we leave their other parameters unchanged, as introduced in the previous consideration.

For this study, we modify our numerical model by adding a second metamolecule to the computation domain in the solver. All calculation procedures related to the multipole expansion method are also reworked to provide decomposition in the local coordinate systems, the origin of which is transferred to the center of mass of the corresponding object, maintaining their “meta-atom→metamolecule→metamacromolecule” hierarchy.

#### B. Secondary multipole decomposition

The main purpose of involving the secondary multipole decomposition (SMD) method is to obtain a representation of the multipole moments of the entire metamacromolecule via the multipole moments of its subsystems. In particular, it allows us to elucidate the physical conditions of the TD resonances as well as their electromagnetic coupling.

The SMD procedure for a cluster of particles bearing the TD moment was introduced in Refs. [37,43]. It has been shown that by using the replacement  $\mathbf{r} = \mathbf{r}_n + \mathbf{r}'_n$  of the

radius-vector  $\mathbf{r}$  defined with respect to the center of mass of the cluster, where  $\mathbf{r}_n$  ( $n = 1 \dots N$ ) are the radius-vectors of the disk's centers and  $\mathbf{r}'_n$  is the radius-vector of any point inside the corresponding disk to its center (see Fig. 9 in Ref. [37]), the vector of the TD moment can be represented as

$$\mathbf{T} = \sum_{n=1}^N \left\{ \mathbf{T}_0(\mathbf{r}_n) + \mathbf{T}_n + \frac{4}{5}[\mathbf{r}_n \times \mathbf{m}_n] + \mathbf{I}(\mathbf{r}_n) \right\}, \quad (5)$$

where

$$\mathbf{T}_0(\mathbf{r}_n) = \frac{\omega}{10i} [(\mathbf{r}_n \cdot \mathbf{p}_n)\mathbf{r}_n - 2r_n^2\mathbf{p}_n] \quad (6)$$

is the TD moment at the cluster mass center associated with the LWA electric dipole moment,

$$\mathbf{p}_n = \frac{i}{\omega} \int_{V_n} \mathbf{J}_D d\mathbf{r}_n,$$

of the subsystem with the number  $n$ ;

$$\mathbf{T}_n = \frac{1}{10} \int_{V_n} [(\mathbf{r}'_n \cdot \mathbf{J}_D)\mathbf{r}'_n - 2(r'_n)^2\mathbf{J}_D] d\mathbf{r}'_n$$

and

$$\mathbf{m}_n = \frac{1}{2} \int_{V_n} [\mathbf{r}'_n \times \mathbf{J}_D] d\mathbf{r}'_n$$

are the TD moment and the LWA MD moment of the subsystem with the number  $n$  calculated with respect to its mass center, respectively; and

$$\mathbf{I}(\mathbf{r}_n) = \frac{1}{10} \int_{V_n} [(\mathbf{r}'_n \cdot \mathbf{J}_D)\mathbf{r}_n - 3(\mathbf{r}_n \cdot \mathbf{J}_D)\mathbf{r}'_n] d\mathbf{r}'_n \quad (7)$$

is an additional integral term that accounts for the offset of the  $n$ th particle from the cluster's mass center.

In order to clarify the role of individual toroidal moments of two subsystems, the use of the method of secondary multipole analysis comes down to considering the complete system as their combination. Therefore, the total multipole moments of the whole system are represented through the multipole moments of its parts, calculated relative to their centers of mass, respectively. Thus, the equations presented in this section should be written taking into account the volumes of only two subsystems.

#### C. Bonding and antibonding eigenstates

As before, here we start with the analysis of eigenstates of the metamacromolecule (Fig. 3). Two corresponding eigenstates are extracted from the set based on the assumption that their eigenfrequencies are located close to the eigenfrequency  $f_{\text{eigen}}$  of the toroidal-like mode of the single metamolecule, while checking the similarity in the distribution of their eigenfields. In these two eigenstates of the metamacromolecule, the dipole-dipole interaction [30] manifests itself in the form of bonding ( $f_{\text{bonding}} \approx 14.31$  GHz) and antibonding ( $f_{\text{antibonding}} \approx 14.45$  GHz) configurations of the electromagnetic coupling, which is also valid for two toroidal-like modes. Similar to other types of dipole-dipole interactions [which can be either electric (ED-ED) or magnetic (MD-MD) type], bonding and antibonding configurations of the toroidal-like

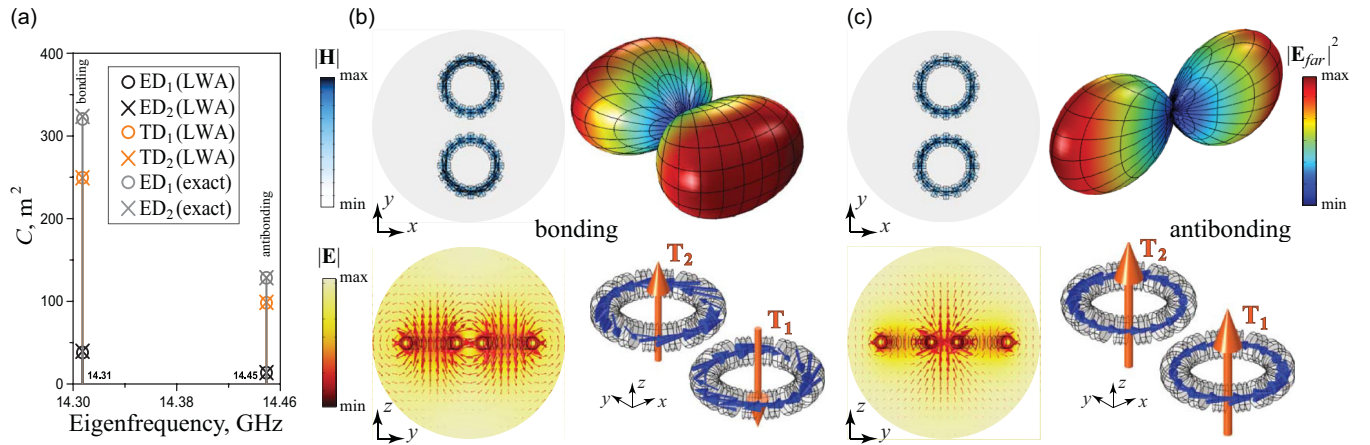


FIG. 3. (a) Contributions of the separate total exact ED moment and ED and TD moments calculated in the LWA for the subsystems to the radiation power of bonding and antibonding eigenstates of the metamacromolecule. The magnitude and flow of the magnetic (cold color map, black arrows) and electric (hot color map, red arrows) near fields, far-field diagram of the metamacromolecule, and schematic representation of the individual MD moments (blue arrows), and TD moments ( $\mathbf{T}_1$  and  $\mathbf{T}_2$ , orange arrows) of its subsystems for the (b) bonding and (c) antibonding eigenstates. All geometric parameters of the metamacromolecule are the same as in Fig. 1, while  $\varepsilon_d = 100$  and  $D = 40$  mm.

modes (TD-TD type) differ in frequency, fulfilling the condition  $f_{\text{bonding}} < f_{\text{antibonding}}$ , i.e., the bonding mode is at lower energy and the antibonding mode is at a higher one, which corresponds to a fundamental physical principle known from the bonding theory [49].

At this stage, we reveal the characteristics of the entire system by considering the behavior of the ED and TD moments of individual rings. Thus, Fig. 3(a) suggests that the magnitude of the individual ED<sub>*j*</sub> and TD<sub>*j*</sub> contributions ( $j = 1, 2$ ) to the radiating eigenfield is higher for the bonding mode compared to the antibonding one, where, in both states, the contributions of the TD moments are still much greater than the ED ones. The peculiarities of the distribution of the electromagnetic near field of these modes cause this difference. In particular, for the bonding mode [Fig. 3(b)], the magnetic field has an antidiagonal circular flow in adjacent rings, which is associated with an antiphase electric field flow in two subsystems that is mainly localized at the centers of the rings. The vectors of the individual TD moments of two rings have only  $z$  components, arising in opposite directions to each other, and a dumbbell-shaped far-field radiation pattern is formed along the  $y$  axis. Contrariwise, for the antibonding mode [Fig. 3(c)], the codirectional flow of the magnetic field in the rings corresponds to the electric field localized in the center of the metamacromolecule. Two in-phase TD moments are located in the center of the corresponding ring, and a dumbbell-shaped radiation pattern is formed along the  $x$  axis. The latter is azimuthally flatter compared to the radiation pattern of the bonding mode. We should note that this difference in electric field localization for the bonding and antibonding modes is an important feature that can be used in practical systems, particularly in biosensors.

Features and differences in the radiation patterns of bonding and antibonding modes can be explained using their symmetry properties. Indeed, from the multipole composition of individual rings of the metamolecule in the bonding and antibonding modes (Fig. 3), it follows that the main multipole contribution corresponds to their exact electric dipole moments. Application of LWA shows that the main contribution

at each exact ED moment corresponds to the toroidal terms. Therefore, a qualitative multipole content of the bonding and antibonding modes can be presented as just two TD moments located at the centers of the rings and directed accordingly (thick orange arrows in Fig. 3). Since for the bonding (antibonding) mode the toroidal dipoles are in antiphase (in phase), it has (does not have) inversion symmetry. Therefore, the multipole moments of the entire metamolecule in the bonding (antibonding) mode should have only positive (negative) parity. As is known [50], the first group of even (positive parity) multipoles of low order includes a magnetic dipole and an electric quadrupole, and therefore the radiation pattern of the bonding mode represents a superposition of magnetic dipole and electric quadrupole radiation. In turn, the radiation pattern for the antibonding mode is determined by the superposition of odd (negative parity) multipole radiation including exact electric dipole, magnetic quadrupole, and electric octupole. Namely, the difference in the multipole composition of radiation from the modes explains the difference in the spatial distribution. Note that in the problem of excitation of bonding and antibonding modes by external waves, analysis of the multipole moments of the entire metamolecule can be used to identify the type of excited mode.

#### D. Bonding and antibonding manifestation

Based on the above-given analysis of eigenstates, one can assume that the excitation of these modes requires different conditions for the irradiating wave. In particular, to excite the bonding and antibonding modes, the metamacromolecule should be irradiated by waves propagated along the  $y$  ( $\mathbf{k} = \{0, k_y, 0\}$ ) and  $x$  ( $\mathbf{k} = \{k_x, 0, 0\}$ ) directions, respectively, while keeping their polarization along the  $z$  axis ( $\mathbf{E} = \{0, 0, E_z\}$ ). The results of our calculations of the characteristics of the scattered field are presented in Fig. 4 for two cases of lateral irradiation of the metamacromolecule, where the multipole contributions are also derived and presented for the entire structure as a whole and its two separate subsystems. They are

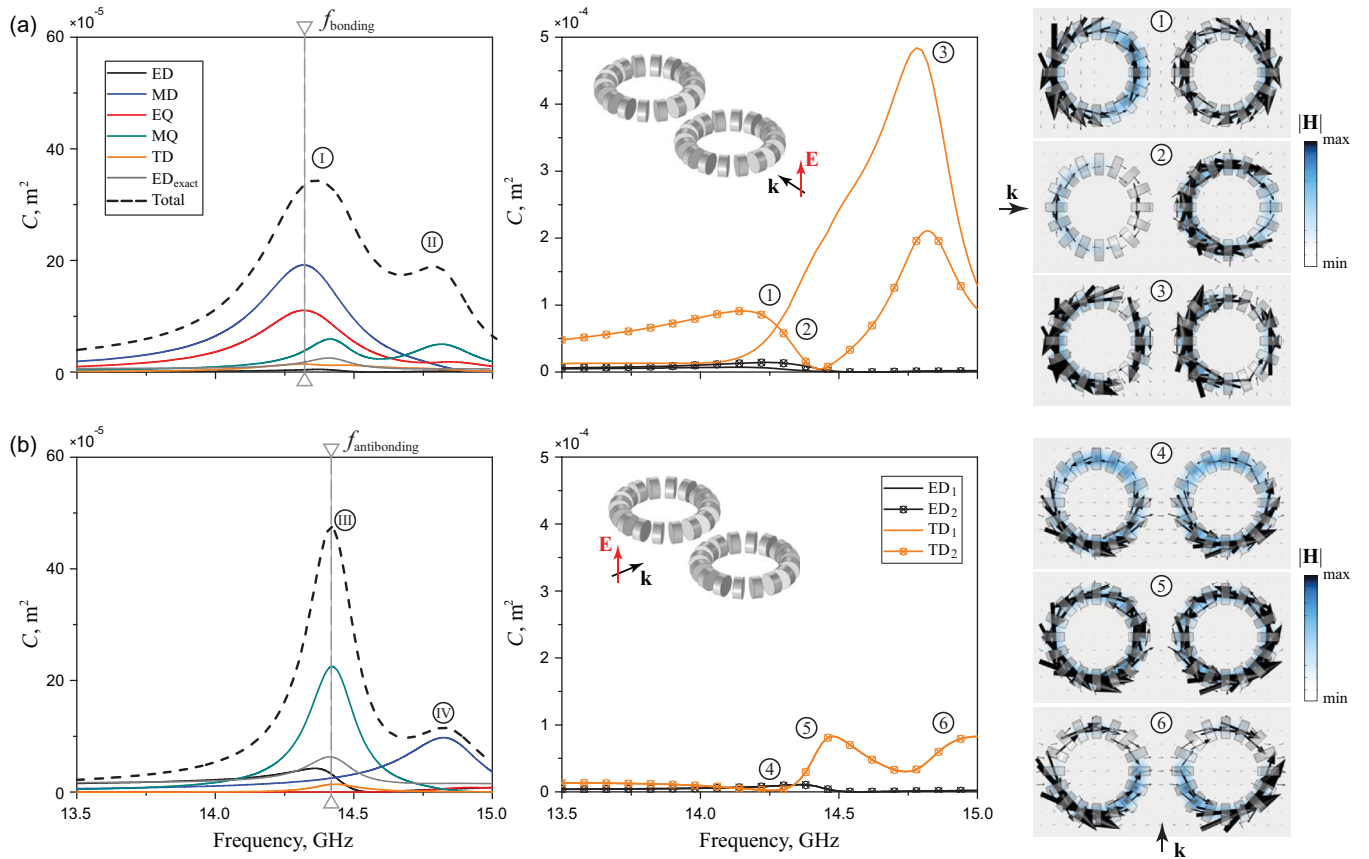


FIG. 4. Manifestation of (a) bonding and (b) antibonding conditions of the electromagnetic coupling of toroidal dipole moments in the scattering cross section of the metamacromolecule. Here, in the first, second, and third columns, the multipole composition of the metamacromolecule, separate ED and TD moments of its subsystems, and the magnetic near-field distributions are given, respectively. The eigenfrequencies of the corresponding modes are indicated by a vertical dashed line. Insets: The direction and polarization of the incident wave. All geometric parameters of the metamacromolecule are the same as in Fig. 3. Here, ①, ④  $f = 14.25$  GHz, ②, ⑤  $f = 14.36$  GHz, and ③, ⑥  $f = 14.78$  GHz.

supplemented by pictures of the magnetic near-field distribution plotted in the horizontal plane of the metamacromolecule (at  $z = 0$ ).

One can see that in the selected frequency range, the scattering characteristics of the metamacromolecule have two pronounced resonances for each excitation condition. For definiteness, we numbered these resonances with encircled Roman numerals ①–④. It is important that resonances ① and ③ are located close to the eigenfrequencies  $f_{\text{bonding}}$  and  $f_{\text{antibonding}}$ , respectively, being manifestations of the corresponding modes of interest, whereas resonances ② and ④ obviously have another origin. Moreover, these spectra clearly show that the antibonding resonance ③ has a higher magnitude (higher energy) and is more narrowband than the bonding one ① (lower energy) as the bonding theory suggests, although both of them arise due to the hybridization of the same toroidal-like modes of individual rings. The multipole decomposition also indicates that the main contribution to resonances ① and ④ comes from a magnetic dipole (MD) and electric quadrupole (EQ), while for resonances ③ and ②, it is a magnetic quadrupole (MQ), which somehow mask their toroidal nature for the observer in the far-field zone. These resonant MD, EQ, and MQ contributions arise in full accordance with the symmetry analysis of the bonding and

antibonding modes presented above and confirm their excitation by external waves.

Moreover, the toroidal nature of the given resonances can also be revealed through the secondary multipole analysis by considering the contributions of individual subsystems to the total scattering cross section of the entire metamacromolecule. In particular, one can conclude that the individual TD contributions of the structure subsystems demonstrate a resonant behavior in the chosen frequency range, the magnitude of which is much greater than the corresponding ED contributions. Since, in the bonding mode excitation, the rings are located in series concerning the direction of propagation of the incident wave, the magnitudes of TD<sub>1</sub> and TD<sub>2</sub> are different. Contrariwise, parallel excitation of the antibonding mode provides the same scattering characteristics for the TD<sub>1</sub> and TD<sub>2</sub> contributions.

To fully reveal the resonant nature of these toroidal contributions, we plot pictures of the magnetic near-field distribution at several specific points selected on the frequency scale. For clarity, we numbered these points with encircled Arabic numerals. At point ①, the magnitudes of the TD<sub>1</sub> and TD<sub>2</sub> contributions are almost the same and the bonding state can be clearly seen in the magnetic field picture. With increasing frequency, the pattern of the magnetic field

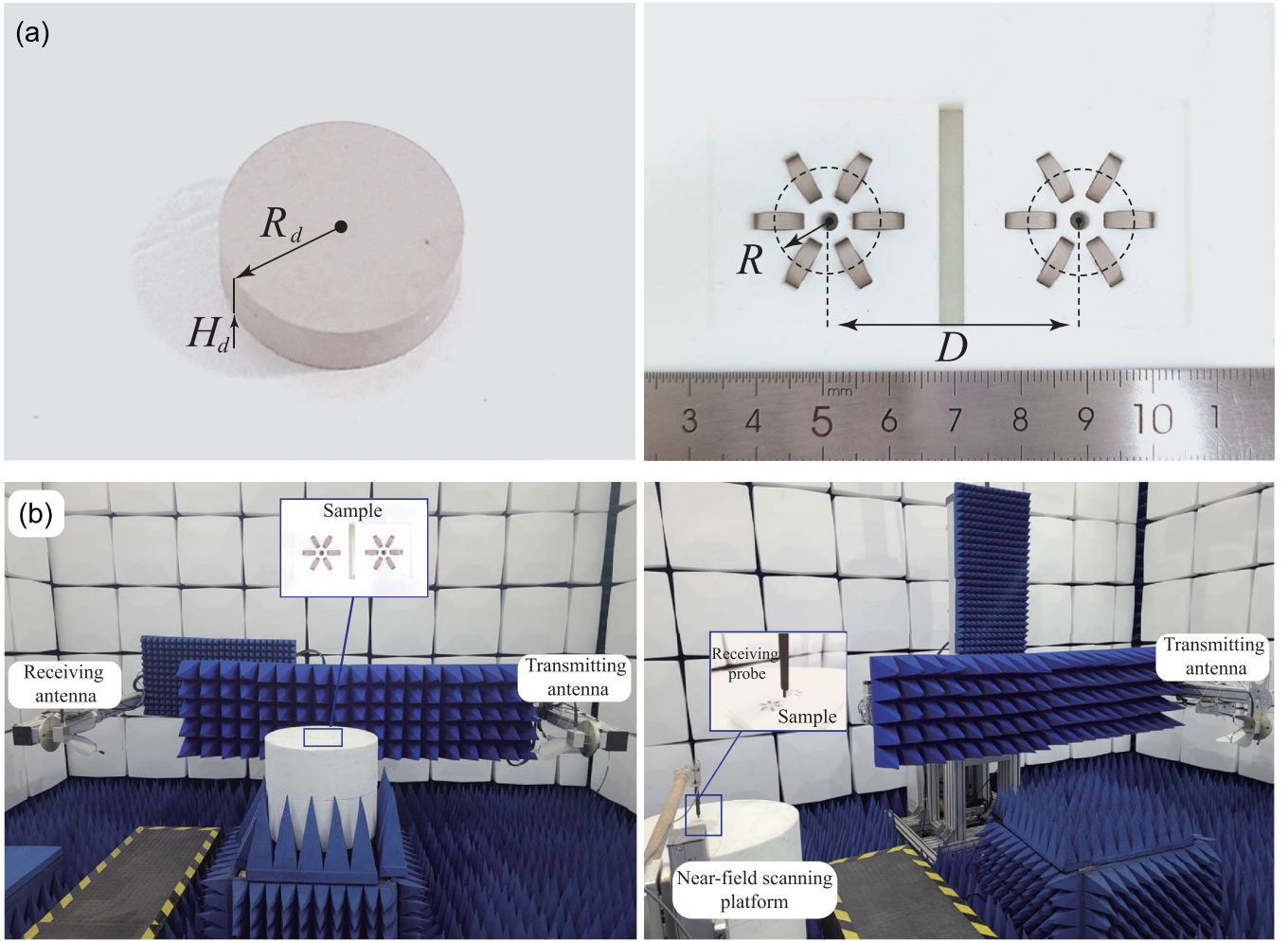


FIG. 5. (a) Actual view and principal dimensions of a single freestanding ceramic resonator (left) and metamacromolecule assembled on a dielectric substrate (right). The disk's radius  $R_d$  and height  $H_d$  are 4.0 and 2.5 mm, respectively. Each toroidal ring consists of  $N = 6$  resonators, the ring's radius  $R$  is  $R_d N / \pi$ , and the distance  $D$  between the center of two rings is 38.0 mm. (b) Photographs of the experimental setup for measurement of the extinction cross section (left) and electromagnetic near-field distribution (right).

distribution changes, appearing as a superposition of two states. In particular, as an additional state contributing to the mode interference, the second-order mode of the torus arises, which is the origin of resonance ⑩ (this mode can be correlated with the toroidal mode of the first type with index  $m = 1$  derived in Ref. [47]) In particular, this second-order mode is characterized by two variations of the magnetic field enclosed in the torus. Regarding the antibonding state, the in-phase behavior of the magnetic field flow is maintained with increasing frequency, where at point ⑥, a resonance of the second-order mode of the torus becomes dominant, which is the origin of resonance ⑨.

The obtained results show that such exotic bonding and antibonding states indeed appear in both the eigen- and scattered spectra of the structure, and, thus, they can be observed experimentally, to which we proceed in the next section.

## IV. EXPERIMENTAL OBSERVATION

### A. Sample and measurement setup

To reveal the peculiarities of the excitation and coupling of toroidal-like modes in the given structures, we prepare

several samples for their microwave characterization [Fig. 5(a)]. The disk-shaped resonators are fabricated from the commercially available Taizhou Wangling TP ceramic by a water jet cutting technique. The relative permittivity of this material declared by the manufacturer is  $\epsilon_d = 22 \pm 1$  and the dissipation factor is  $\tan \delta = 1 \times 10^{-3}$  referenced to the frequency of 10 GHz. Although the parameters of the ceramic material turned out to be lower than expected for our experiment, the permittivity and dimensions of the produced resonators still allow us to study the manifestation of the TD modes in the experimental structures. Since the permittivity of the disks is not large compared to that considered in the previous numerical sections, the radius of the torus for experimental structures was reduced to satisfy the long-wavelength approximation conditions. In turn, reducing the radius required reducing the number of resonators used to form the ring. Therefore, each toroidal ring of the experimental metamacromolecule consists of  $N = 6$  vertically standing disks fixed on an airtight dielectric substrate. This substrate is made from the Rohacell HF rigid foam plate. The relative permittivity of the foam is  $\epsilon_s = 1 \pm 0.1$ . A high-precision milling machine, Roland

MDX-50, was used to process the foam substrate to fix the resonators in the corresponding seats.

A bistatic method is carried out to measure an extinction cross section (ECS) of samples. During the measurement, the sample is positioned between two horn antennas (GuanJun GJ-WDRHA-1/18-3/13-S) operating to generate and receive a linearly polarized wave [Fig. 5(b)]. They are mounted on the corresponding robotic arms of the measurement setup. Antennas are connected to corresponding ports of the vector network analyzer (VNA) Rohde & Schwarz ZVA-50 (the operating principle and dynamic range of the analyzer can be found elsewhere [51,52]). The antennas are oriented in such a way that the electric field vector of the transmitted wave is oriented vertically (along the  $z$  axis). The sample is placed on a height-adjustable table, which is fixed at the geometrical center point of the arms assembly. The distance from the edge of each antenna to the center of the sample is set at approximately 1.5 m, which satisfies the far-field radiation conditions.

The  $S_{21}$  coefficient of the electromagnetic waves passing through the sample (one ring, two rings, and free space) is recorded by the VNA. The measurement of wave transmission through free space (i.e., without any sample) is utilized as a reference signal. The forward scattering is then calculated as the difference between the  $S_{21}$  coefficient measured for the sample and free space. The magnitude and phase of the  $S_{21}$  coefficient are collected in the frequency range of 7–9 GHz. This range is determined from corresponding numerical simulations performed in the solver for actual structures. The ECS is extracted from the complex  $S_{21}$  magnitude through the optical theorem [53,54].

After obtaining the scattered spectra, the samples are subjected to measurement of their near-field characteristics at the corresponding resonant frequencies. For the near-field characterization, a single antenna is connected to the first port of the VNA to illuminate the sample, and either an electric (Hertz) or magnetic (loop) dipole is connected to another port of the VNA as a receiving probe to measure the spatial distribution of the corresponding near-field components. Depending on the need, the probe can be oriented in such a way as to measure either vertical or horizontal components of the electromagnetic near field. The scanning area of the pattern is  $100 \times 100 \text{ mm}^2$ , and the Linbou near-field imaging system is used to move the probe in the vertical and horizontal directions above the sample with a step of 2 mm. The corresponding probe is fixed with a low permittivity holder to the wooden arm of the imaging system during the experiment. Measurements can be carried out in the upper hemisphere from a certain distance from the structure's surface. This distance is set to 1 mm. All measurements are performed in an anechoic chamber.

To support our experiment, we modified our numerical model in the COMSOL solver. We conducted additional numerical simulations to calculate the ECS and electromagnetic near-field distribution for the actual structures, accounting for the material losses present in their constitutive ceramics.

### B. Measurement results

The simulation and measurement results of the near fields for a single ring and a system of two rings are collected in

Fig. 6. One can notice that the measured results correspond well with the simulated ones. It confirms that the toroidal-like mode can indeed be excited in structures with actual material losses by the external waves with proper polarization.

In particular, the real part of the  $z$  component of the electric near field is mapped in the horizontal ( $x$ - $y$ ) plane for a single ring and a pair of rings operated in the antibonding mode. One can see that the resulting patterns have a very similar appearance, where the ring-shaped distribution of the field can be easily observed, thus confirming the toroidal nature of the excited resonances. However, for the excitation condition of the bonding state, the pattern of the  $E_z$  component appears to be somewhat uncertain. The obtained results indicate that the interference effect identified earlier [see point ② in Fig. 4(a)] contributes to the resulting picture. The resulting uncertainty in the pattern for the bonding resonance is also aggravated by the fact that the data for the electric near field are collected at some distance above the structure, while a clear interpretation is possible only in the  $z = 0$  plane, which is a physically inaccessible region for direct measurements. This uncertainty required an additional measurement of the real part of the  $x$  component of the magnetic near field in the vertical ( $y$ - $z$ ) plane. The difference in the intensity of the  $H_x$  component between the centers of the two rings indicates the opposite flow of the magnetic near field, which indirectly confirms the emergence of the bonding mode in the structure. Therefore, the obtained results are in good agreement with the results of the numerical model, thus generally confirming the conditions for the existence of a bonding mode in the structure.

### V. CONCLUSIONS

In summary, we have studied, both numerically and experimentally, a manifestation of the toroidal-like mode in a single ring consisting of several dielectric disks. We determine the mode from the solution to the eigenvalue problem of the system by considering the conditions of the eigenfield and performing the multipole expansion. Then, the characteristics of a system composed of two identical rings are studied in the eigen- and excited states to reveal the peculiarities of the toroidal dipole coupling.

The manifestation of the toroidal-like mode and its electromagnetic coupling is verified on the samples made from ceramic particles irradiated by a linearly polarized wave by measuring the far-field and near-field characteristics of the scattered waves. While the experimental and numerical results agree very well and both bonding and antibonding states are observed, there is some undesirable field distortion obtained in the experiment. This distortion is caused by the fact that the structure's size is almost comparable to the length of the incident wave, which somewhat violates the conditions of the long-wavelength approximation where the toroidal dipole is unambiguously defined.

Revealing the nature of toroidal moments is important from the point of view of fundamental physics. It is possible to construct a special theory of the toroidal-like interaction, in the same way as it is done for other types of interactions (e.g., electric charge-dipole, electric dipole-dipole, magnetic dipole-dipole), taking into account that the toroidal dipole cannot be considered as a point source. Also, we expect our

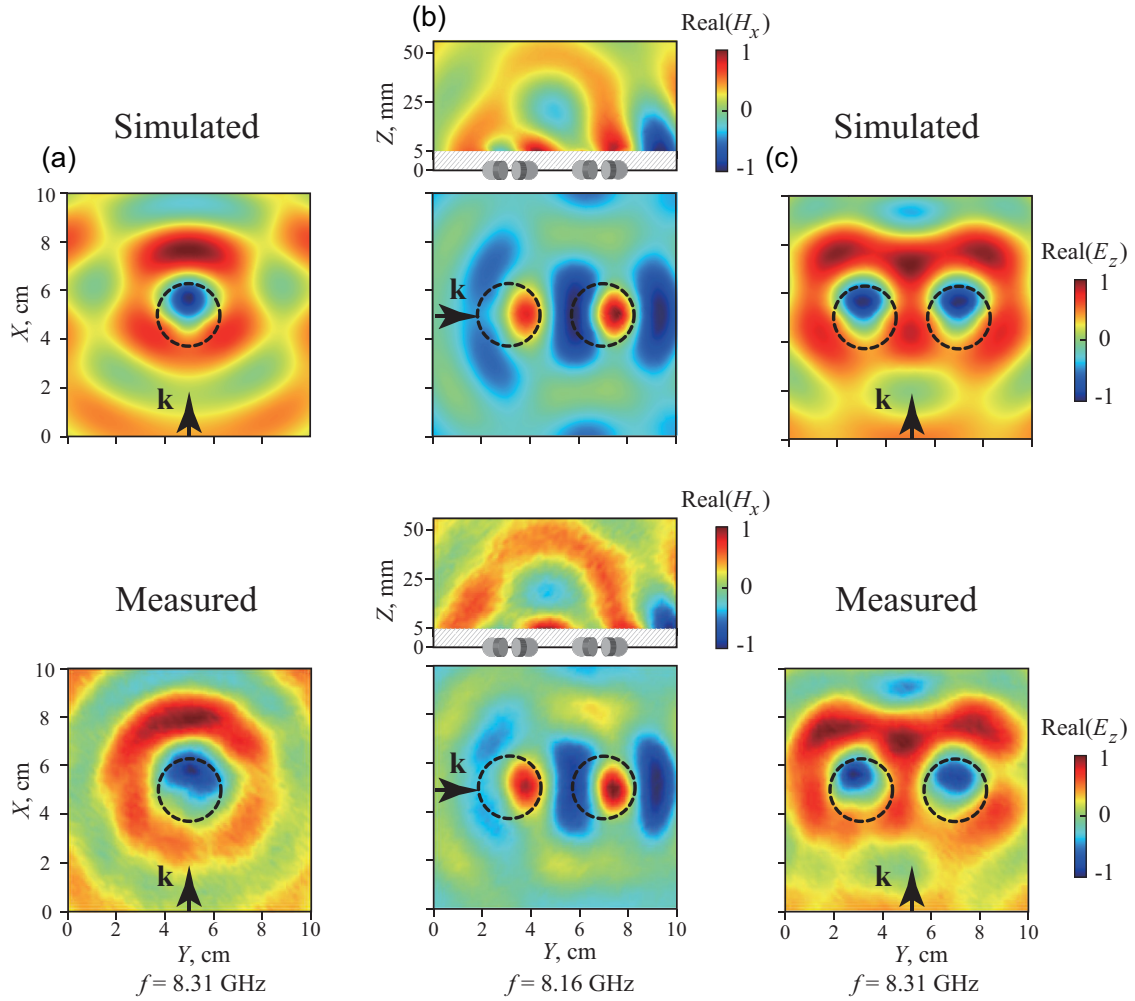


FIG. 6. Simulated (upper row) and measured (bottom row) distributions of the electromagnetic near field (real part) for structures comprising (a) one ring and two rings, irradiated to excite (b) bonding and (c) antibonding states. All patterns are normalized on the corresponding maximal values. The real parts of the  $H_x$  and  $E_z$  components are plotted in the  $y$ - $z$  (rectangular areas) and  $x$ - $y$  (square areas) planes. Hatching marks an area that is physically inaccessible for direct measurement. The parameters of the structures are the same as indicated in the caption to Fig. 5.

results to be important for practical applications when designing new photonic devices, particularly lasers and biosensors.

#### ACKNOWLEDGMENTS

T.W. and V.R.T. are grateful for the support from Jilin University, China. A.B.E. is thankful for funding support from the Deutsche Forschungsgemeinschaft (DFG, German Research Foundation) under Germany's Excellence Strategy within the Cluster of Excellence PhoenixD (Grant No. 390833453).

#### APPENDIX: ELECTRIC FIELDS OF ELECTRIC AND TOROIDAL DIPOLE MOMENTS

The electric field created by oscillating electric  $\mathbf{p}$  and toroidal  $\mathbf{T}$  dipole moments localized at point  $\mathbf{r}'$  of free space can be represented in the following form [55,56]:

$$\mathbf{E}^p(\mathbf{r}) = \frac{k_0^2}{\varepsilon_0} \hat{G}(\mathbf{r}, \mathbf{r}') \mathbf{p} \quad (\text{A1})$$

and

$$\mathbf{E}^T(\mathbf{r}) = i \frac{k_0^2}{c \varepsilon_0} \hat{G}(\mathbf{r}, \mathbf{r}') \mathbf{T}, \quad (\text{A2})$$

where the Green tensor is

$$\hat{G}(\mathbf{r}, \mathbf{r}') = \left\{ \left( 1 + \frac{i}{k_0 R} - \frac{1}{k_0^2 R^2} \right) \hat{U} + \left( -1 - \frac{3i}{k_0 R} + \frac{3}{k_0^2 R^2} \right) \mathbf{nn} \right\} \frac{e^{ik_0 R}}{4\pi R}, \quad R \neq 0, \quad (\text{A3})$$

$R = |\mathbf{r} - \mathbf{r}'|$ ,  $\mathbf{n} = (\mathbf{r} - \mathbf{r}')/R$ , and  $\hat{U}$  is the  $(3 \times 3)$  unit tensor. From the representations (A1) and (A2), it follows that in the static limit  $k_0 \rightarrow 0$ ,

$$\mathbf{E}^p(\mathbf{r}) = (-\hat{U} + 3\mathbf{nn}) \frac{\mathbf{p}}{4\pi \varepsilon_0 R^3}, \quad \mathbf{E}^T(\mathbf{r}) = 0. \quad (\text{A4})$$

It is interesting to note that the vector potential  $\mathbf{A}^T(\mathbf{r})$  of a toroidal dipole in the static case is not zero and completely repeats the spatial distribution of the electric

field of the static electric field [55,57]. Therefore, the radiation diagram and spatial distribution of electromagnetic fields of the TD moment follow the same configuration as that of the ED moment. However, the similarity with the

distribution of the fields generated by ED and TD disappears when approaching the static limit. Unlike a static ED, a static TD does not generate fields but creates a nonzero vector potential.

- 
- [1] A. R. Leach, *Molecular Modelling: Principles and Applications*, 2nd ed. (Pearson Prentice Hall, Harlow, 2009).
- [2] T. J. Cui, D. R. Smith, and R. Liu, *Metamaterials: Theory, Design, and Applications* (Springer, New York, 2010).
- [3] W. Cai and V. M. Shalae, *Optical Metamaterials: Fundamentals and Applications* (Springer, New York, 2010).
- [4] A. Sihvola, Metamaterials in electromagnetics, *Metamaterials* **1**, 2 (2007).
- [5] J. B. Pendry, A. J. Holden, D. J. Robbins, and W. J. Stewart, Magnetism from conductors and enhanced nonlinear phenomena, *IEEE Trans. Microwave Theory Tech.* **47**, 2075 (1999).
- [6] A. B. Evlyukhin, S. M. Novikov, U. Zywiets, R. L. Eriksen, C. Reinhardt, S. I. Bozhevolnyi, and B. N. Chichkov, Demonstration of magnetic dipole resonances of dielectric nanospheres in the visible region, *Nano Lett.* **12**, 3749 (2012).
- [7] A. I. Kuznetsov, A. E. Miroshnichenko, Y. H. Fu, and B. Zhang, J. Luk'yanchuk, Magnetic light, *Sci. Rep.* **2**, 492 (2012).
- [8] F. Monticone and A. Alù, The quest for optical magnetism: from split-ring resonators to plasmonic nanoparticles and nanoclusters, *J. Mater. Chem. C* **2**, 9059 (2014).
- [9] M. Fiebig, Revival of the magnetoelectric effect, *J. Phys. D: Appl. Phys.* **38**, R123 (2005).
- [10] T. Kaelberer, V. A. Fedotov, N. Papasimakis, D. P. Tsai, and N. I. Zheludev, Toroidal dipolar response in a metamaterial, *Science* **330**, 1510 (2010).
- [11] V. Savinov, V. A. Fedotov, and N. I. Zheludev, Toroidal dipolar excitation and macroscopic electromagnetic properties of metamaterials, *Phys. Rev. B* **89**, 205112 (2014).
- [12] A. A. Basharin, M. Kafesaki, E. N. Economou, C. M. Soukoulis, V. A. Fedotov, V. Savinov, and N. I. Zheludev, Dielectric metamaterials with toroidal dipolar response, *Phys. Rev. X* **5**, 011036 (2015).
- [13] V. R. Tuz, V. V. Khardikov, and Y. S. Kivshar, All-dielectric resonant metasurfaces with a strong toroidal response, *ACS Photon.* **5**, 1871 (2018).
- [14] S. Xu, A. Sayanskiy, A. S. Kupriyanov, V. R. Tuz, P. Kapitanova, H.-B. Sun, W. Han, and Y. S. Kivshar, Experimental observation of toroidal dipole modes in all-dielectric metasurfaces, *Adv. Opt. Mater.* **7**, 1801166 (2019).
- [15] N. A. Spaldin, M. Fiebig, and M. Mostovoy, The toroidal moment in condensed-matter physics and its relation to the magnetoelectric effect, *J. Phys.: Condens. Matter* **20**, 434203 (2008).
- [16] V. M. Dubovik and V. V. Tugushev, Toroid moments in electrodynamics and solid-state physics, *Phys. Rep.* **187**, 145 (1990).
- [17] X.-L. Li and J. Tang, Recent developments in single-molecule toroids, *Dalton Trans.* **48**, 15358 (2019).
- [18] N. Papasimakis, V. A. Fedotov, V. Savinov, T. A. Raybould, and N. I. Zheludev, Electromagnetic toroidal excitations in matter and free space, *Nat. Mater.* **15**, 263 (2016).
- [19] N. Talebi, S. Guo, and P. A. van Aken, Theory and applications of toroidal moments in electrodynamics: their emergence, characteristics, and technological relevance, *Nanophotonics* **7**, 93 (2018).
- [20] M. Gupta, K. Y. Srivastava, M. Manjappa, and R. Singh, Sensing with toroidal metamaterial, *Appl. Phys. Lett.* **110**, 121108 (2017).
- [21] A. Ahmadivand, B. Gerislioglu, R. Ahuja, and Y. Kumar Mishra, Terahertz plasmonics: The rise of toroidal metadevices towards immunobiosensings, *Mater. Today* **32**, 108 (2020).
- [22] Y.-W. Huang, W. T. Chen, P. C. Wu, V. A. Fedotov, N. I. Zheludev, and D. P. Tsai, Toroidal lasing spaser, *Sci. Rep.* **3**, 1237 (2013).
- [23] I. Fernandez-Corbaton, S. Nanz, and C. Rockstuhl, On the dynamic toroidal multipoles from localized electric current distributions, *Sci. Rep.* **7**, 7527 (2017).
- [24] R. Alae, C. Rockstuhl, and I. Fernandez-Corbaton, An electromagnetic multipole expansion beyond the long-wavelength approximation, *Opt. Commun.* **407**, 17 (2018).
- [25] A. Ospanova, M. Cojocari, and A. Basharin, Modified multipoles in photonics, *Phys. Rev. B* **107**, 035156 (2023).
- [26] A. Canós Valero, D. Borovkov, A. Kalganov, A. Dudnikova, M. Sidorenko, P. Dergachev, E. Gurvitz, L. Gao, V. Bobrov, A. Miroshnichenko, and A. S. Shalin, On the existence of pure, broadband toroidal sources in electrodynamics, *Laser Photon. Rev.* **18**, 2200740 (2024).
- [27] S. Nanz, *Toroidal Multipole Moments in Classical Electrodynamics: An Analysis of Their Emergence and Physical Significance*, BestMasters (Springer, Fachmedien Wiesbaden, 2016).
- [28] E. A. Gurvitz, K. S. Ladutenko, P. A. Dergachev, A. B. Evlyukhin, A. E. Miroshnichenko, and A. S. Shalin, The high-order toroidal moments and anapole states in all-dielectric photonics, *Laser Photon. Rev.* **13**, 1800266 (2019).
- [29] R. S. Mulliken, Chemical bonding, *Annu. Rev. Phys. Chem.* **29**, 1 (1978).
- [30] W. Rechberger, A. Hohenau, A. Leitner, J. R. Krenn, B. Lamprecht, and F. R. Aussenegg, Optical properties of two interacting gold nanoparticles, *Opt. Commun.* **220**, 137 (2003).
- [31] P. Nordlander, C. Oubre, E. Prodan, K. Li, and M. I. Stockman, Plasmon hybridization in nanoparticle dimers, *Nano Lett.* **4**, 899 (2004).
- [32] E. Prodan, C. Radloff, N. J. Halas, and P. Nordlander, A hybridization model for the plasmon response of complex nanostructures, *Science* **302**, 419 (2003).
- [33] S. K. Ghosh and T. Pal, Interparticle coupling effect on the surface plasmon resonance of gold nanoparticles: From theory to applications, *Chem. Rev.* **107**, 4797 (2007).
- [34] A. E. Miroshnichenko, B. Luk'yanchuk, S. A. Maier, and Y. S. Kivshar, Optically induced interaction of magnetic moments in hybrid metamaterials, *ACS Nano* **6**, 837 (2012).
- [35] A. E. Miroshnichenko, D. Filonov, D. Lukyanchuk, and Y. Kivshar, Antiferromagnetic order in hybrid electromagnetic metamaterials, *New J. Phys.* **19**, 083013 (2017).

- [36] V. R. Tuz, P. Yu, V. Dmitriev, and Y. S. Kivshar, Magnetic dipole ordering in resonant dielectric metasurfaces, *Phys. Rev. Appl.* **13**, 044003 (2020).
- [37] V. R. Tuz, V. Dmitriev, and A. B. Evlyukhin, Antitoroidic and toroidic orders in all-dielectric metasurfaces for optical near-field manipulation, *ACS Appl. Nano Mater.* **3**, 11315 (2020).
- [38] V. Dmitriev, A. S. Kupriianov, S. D. S. Santos, and V. R. Tuz, Symmetry analysis of trimer-based all-dielectric metasurfaces with toroidal dipole modes, *J. Phys. D: Appl. Phys.* **54**, 115107 (2021).
- [39] V. Dmitriev, Silvio Domingos Silva Santos, A. B. Evlyukhin, A. S. Kupriianov, and V. R. Tuz, Toroidic and antitoroidic orders in hexagonal arrays of dielectric trimers: Magnetic group approach, *Phys. Rev. B* **103**, 165402 (2021).
- [40] V. Dmitriev, S. D. S. Santos, A. S. Kupriianov, and V. R. Tuz, Transition between toroidic orders in dielectric metasurfaces by polarization of the incident wave, *Opt. Lett.* **46**, 2964 (2021).
- [41] V. R. Tuz, A. B. Evlyukhin, and V. I. Fesenko, Transition between radial and toroidal orders in a trimer-based magnetic metasurface, *Phys. Rev. Appl.* **20**, 044024 (2023).
- [42] Y. V. Kopaev, Toroidal ordering in crystals, *Phys. Usp.* **52**, 1111 (2009).
- [43] V. R. Tuz and A. B. Evlyukhin, Polarization-independent anapole response of a trimer-based dielectric metasurface, *Nanophotonics* **10**, 4373 (2021).
- [44] K. Marinov, A. D. Boardman, V. A. Fedotov, and N. Zheludev, Toroidal metamaterial, *New J. Phys.* **9**, 324 (2007).
- [45] A. B. Evlyukhin and B. N. Chichkov, Multipole decompositions for directional light scattering, *Phys. Rev. B* **100**, 125415 (2019).
- [46] S. Yushanov, J. S. Crompton, and K. C. Koppenhoefer, Mie scattering of electromagnetic waves, in *Proceedings of the COMSOL Conference* (Cosmol Inc., Boston, 2013).
- [47] F. Cap and R. Deutsch, Toroidal resonators for electromagnetic waves, *IEEE Trans. Microwave Theory Tech.* **26**, 478 (1978).
- [48] R. K. Mongia and P. Bhartia, Dielectric resonator antennas—A review and general design relations for resonant frequency and bandwidth, *Intl. J. RF Microw. Comput. Aided Eng.* **4**, 230 (1994).
- [49] L. Pauling, *The Nature of the Chemical Bond*, 3rd ed. (Cornell University Press, Ithaca, NY, 1960).
- [50] M. Poleva, K. Frizyuk, K. Baryshnikova, A. Evlyukhin, M. Petrov, and A. Bogdanov, Multipolar theory of bianisotropic response of meta-atoms, *Phys. Rev. B* **107**, L041304 (2023).
- [51] Rohde & Schwarz, [www.rohde-schwarz.com](http://www.rohde-schwarz.com).
- [52] P. Goy and M. Gross, Millimeter- and submillimeter-wave vector measurements, in *Millimeter and Submillimeter Waves IV*, edited by M. N. Afsar (SPIE, San Diego, CA, 1998), Vol. 3465, pp. 288–303.
- [53] R. G. Newton, Optical theorem and beyond, *Am. J. Phys.* **44**, 639 (1976).
- [54] M. J. Berg, C. M. Sorensen, and A. Chakrabarti, Extinction and the optical theorem. Part I. Single particles, *J. Opt. Soc. Am. A* **25**, 1504 (2008).
- [55] V. A. Fedotov, A. V. Rogacheva, V. Savinov, D. P. Tsai, and N. I. Zheludev, Resonant transparency and nontrivial nonradiating excitations in toroidal metamaterials, *Sci. Rep.* **3**, 2967 (2013).
- [56] A. B. Evlyukhin, T. Fischer, C. Reinhardt, and B. N. Chichkov, Optical theorem and multipole scattering of light by arbitrarily shaped nanoparticles, *Phys. Rev. B* **94**, 205434 (2016).
- [57] G. N. Afanasiev and Y. P. Stepanovsky, The electromagnetic field of elementary time-dependent toroidal sources, *J. Phys. A: Math. Gen.* **28**, 4565 (1995).